Organic Electronics 37 (2016) 55–60

Contents lists available at ScienceDirect

Organic Electronics

journal homepage: www.elsevier.com/locate/orgel

Letter

Characterization of LSMO/C_{60} spinterface by first-principle calculations

E.A. Kovaleva [a, b, *], A.A. Kuzubov [a, b], P.V. Avramov [c], A.V. Kuklin [a, c], N.S. Mikhaleva [a, b], P.O. Krasnov [a, d]

[a] Siberian Federal University, 79 Svobodny pr., Krasnoyarsk, 660041, Russia
[b] L.V. Kirensky Institue of Physics, 50 Akademgorodok, Krasnoyarsk, 660036, Russia
[c] Kyungpook National University, 80 Daekharo, Bukgu, Daegu, 41556, South Korea
[d] Siberian State Technological University, 82 Mira pr., Krasnoyarsk, 660049, Russia

ARTICLE INFO

Article history:
Received 5 April 2016
Received in revised form
8 June 2016
Accepted 14 June 2016
Available online 21 June 2016

Keywords:
C_{60}
LSMO
Spinterface
DFT
Magnetic ordering

ABSTRACT

Spinterface between fullerene C_{60} and $La_{0.7}Sr_{0.3}MnO_3$ (LSMO) was studied by means of density functional theory. Co-existence of many different configurations was shown, and probabilities of their appearance were estimated. Dependence of composite properties on configuration and temperature was also investigated. Key role of transition metal atoms in both binding between composite compartments and magnetic ordering in C_{60} molecule was discussed. The latter was suggested to be responsible for spin-polarized charge transport while overall magnetic moment of fullerene molecule is relatively small.
© 2016 Elsevier B.V. All rights reserved.

1. Introduction

Organic semiconductors are well-known as promising candidates for spintronics due to weak spin-orbit and hyperfine interaction [1–4]. Both giant magnetoresistance effect (GMR) and tunneling magnetoresistance (TMR) effect were observed in organic-based spin valves with rubrene, pentacene, tris(8-hydroxyquinolino) aluminum (Alq_3) and C_{60} as spacers [3,5–10]. Fullerene C_{60} is considered to be especially promising due to the absence of atoms other than carbon and, hence, weaker hyperfine interaction [10–13]. Half-metallic $La_{0.7}Sr_{0.3}MnO_3$ (LSMO) is widely used in spintronic devices due to its high spin polarization [7,11–14] even though it may vary due to the *k* broadening in direction perpendicular to the surface [15] resulting in reduction of spin polarization observed in experiment [16]. It has a lot of advantages comparing with conventional ferromagnetic materials (e.g. Fe, Co, Ni) being much less spin polarized and suffering from well-known conductivity mismatch problem. One way to solve this problem is to add tunnel barriers between FM electrodes and a spacer at the cost of increasing device complexity. Using half-metallic electrodes (LSMO) allows achieving up to the 95% contact spin polarization in MTJ devices without using any additional layers. Moreover, in contrast to abovementioned transition metals, LSMO is highly resistive against oxidation [1]. These features make LSMO an ideal candidate for using in spintronics. Detailed studies of magnetoresistance in LSMO/C_{60}/Co vertical spin valve [11–14,17] including effects of spacer thickness and surface morphology reveal very complex behavior combining GMR resulted from spin injection and TMR due to the presence of pinholes in organic spacer [12]. Magnetoresistance effect was found to increase drastically when C_{60} layer possesses higher crystallinity and larger grain size with many pinholes. Co then can diffuse through these pinholes reducing the effective thickness of spacer and causing tunneling rather than spin injection [12]. In contrast to that, samples with smoother C_{60} surface demonstrate completely different characteristics corresponding to the spin-polarized injection [12]. In order to prevent Co from diffusing into the pinholes, more complex LSMO/C_{60}/AlO_x/Co devices were fabricated [11]. Aluminum oxide was found to suppress cobalt diffusion into the spacer layer effectively. Surprisingly, magnetoresistance effect changes its polarity in this

* Corresponding author. Siberian Federal University, 79 Svobodny pr., Krasnoyarsk, 660041, Russia.
E-mail address: kovaleva.evgeniya1991@mail.ru (E.A. Kovaleva).

http://dx.doi.org/10.1016/j.orgel.2016.06.021
1566-1199/© 2016 Elsevier B.V. All rights reserved.

case becoming positive instead of negative for original LSMO/C_{60}/Co. This is explained in terms of competition between positive GMR channel and pinhole channel in latter case while positive MR dominating in former one [11]. Effect of Co/fullerene spinterface is also investigated both experimentally and theoretically by Liang et al. [14]. However, the nature of interface between C_{60} and LSMO is relatively less investigated. Experimental study of its electronic structure by photoelectron spectroscopy was performed very recently [18]. Shift of HOMO and LUMO levels leading to n-p transition was observed when increasing the thickness of C_{60}. This was attributed to p-doping caused by oxygen diffusion from LSMO to the C_{60} layer.

The present work is originally to study spin polarization features of LSMO/C_{60} hybrid structures by means of density functional theory. When performing DFT calculations, we found many possible structures to be stable revealing the existence of microstates continuously transforming to each other by fullerene's rotation along the surface. Thus, this effect is also to be described in details.

2. Computational details

The first-principles density functional theory calculations of LSMO/C_{60} composites were performed using VASP code [19–22]. GGA PBE potential [23,24] with taking into account Hubbard corrections (GGA + U) [25,26] and projector augmented wave [27,28] method (PAW) were implemented. D3 Grimme correction of weak dispersion interactions [29] was used in order to describe the interaction between fullerene molecule and LSMO substrate correctly. The U = 2 and J = 0.7 eV parameters of GGA + U approach are adopted from earlier calculations of LSMO [30–32]. Geometry optimization was performed until the forces acting on atoms were less than 0.01 eV/Å.

First, unit cell of bulk LSMO was optimized, and the a translation vector is found to be equal to 3.886 Å which is in a good agreement with experimental data (a = 3.876 Å [33] and a = 3.87 Å [34]) and previous theoretical calculations (a = 3.89 Å) [30]. Then, LSMO (001) surface was constructed by cutting it along the corresponding crystallographic plane. Mn-O terminated surface was chosen since it was investigated in experimental works [11–13]. 4 × 4 × 1 supercell of LSMO surface was used for calculation of interface with C_{60}. This means that, in periodic boundary conditions, fullerene molecules are distant from each other (distance between them is ~8.6 Å) and can be considered as isolated. We suppose that mainly the topmost Mn-O layer should be responsible for interface properties so one can use an oversimplified model of 1 unit cell along *c* direction without any cost at computational accuracy while considerably increasing the speed of calculation. Artificial interactions in periodic boundary conditions were avoided by setting the vacuum interval of approximately 13 Å in direction normal to the interface. Lattice vectors were then set to be a = b = 15.544 Å, c = 30.000 Å. The Mönkhorst-Pack [35] k-point Brilloin sampling was used. The k-point grid contained 2 × 2 × 1 points along *a*, *b* and *c* directions, respectively. The energy cut-off was specified as 450 eV in all calculations.

Energy of bonding between fullerene and LSMO slab was estimated as:

$$E_b = E_c - E_f - E_{LSMO}, \quad (1)$$

where E_c, E_f and E_{LSMO} are total energies of composite, fullerene and LSMO slab, respectively. Charge and magnetic moment on fullerene molecule were estimated according to the Bader charge analysis [36–38].

3. Results and discussion

Different possible configurations of LSMO/C_{60} nanocomposite were considered (see Fig. 1). Each configuration is denoted as X(η^y), where X = O or Mn, and y stands for the number of carbon atoms surrounding X (see Fig. 1). Five initial configurations with y varying from 2 to 6 were chosen for Mn-coordinated structures, and, similarly, for O-coordinated ones. Since there are two unequal η^2 configurations (with carbon bond between two hexagons or between hexagon and pentagon placed upon corresponding LSMO atoms), they were designated as η^2 and $\eta^{2'}$, respectively. Obviously, there is no way to construct an η^4 configuration with four carbon atoms being equally distant from coordinating atom. Thus, it has been excluded from the scope of our investigation, and so the total number of initial structures became 10. According to our calculations, binding energies of all structures are considerably high and differ from each other in range of 0.3 eV. Such proximity witnesses the co-existence of many microstates that can easily transform from one to another (see Fig. 1). The height of migration barrier is conditioned mainly by the difference in binding energies. Possibility of fullerene's migration along the surface was also recently reported for Au and Fe surfaces [39,40]. The probability of each state appearance was estimated according to the Gibbs distribution:

$$P_i = \frac{e^{-\frac{E_i}{k_B T}}}{\sum_{i=1}^{10} e^{-\frac{E_i}{k_B T}}} \quad (2)$$

in the temperature range of 300–600 K O(η^3) and O(η^5) were found to be the most probable to occur at 300 K. It can be noticed from Fig. 1 that these two structures possess carbon atoms placed upon Mn atom, while structure with C–C bond upon the Mn atom are less favorable, and ones without contact with manganese atom are considerably higher in energy. This reveals the key role of transition metal atom in binding between LSMO and C_{60} molecule. At the same time, the presence of oxygen leads to repulsion with fullerene's π-conjugated system. Supply from O(η^6) and Mn($\eta^{2'}$) configurations becomes valuable as the temperature increases (18 and 10% at 600 K, respectively, see Table 1). Less pronounced are supplies from O($\eta^{2'}$) and Mn(η^2) (6% at 600 K). Probabilities of other configurations appearance are less than 5% even at 600 K. The analysis of composites' electronic structure (see Table 1) shows that charge and magnetic moment on fullerene molecule is virtually the same for all configurations. Spin polarization at Fermi level was calculated as:

$$\xi = \frac{n_\uparrow - n_\downarrow}{n_\uparrow + n_\downarrow}, \quad (3)$$

where $n_\uparrow$ and $n_\downarrow$ are spin-up and spin-down electron densities at Fermi level, respectively. This value varies from 4 to 22% for different configuration. However, it doesn't change its sign (see Table 1) that means that spin-polarized transport is possible even if one configuration moves to another. Averaged properties of fullerene molecule in LSMO/C_{60} composite were calculated taking into account probabilities of microstates' appearance at different temperatures:

$$X = P_i \cdot X_i, \quad (4)$$

where X is the property, i denotes the configuration, and P is the probability of its appearance at the corresponding temperature. All properties discussed here remain stable in the temperature range of 300–600 K (see Table 2). C_{60} molecule gains the charge of

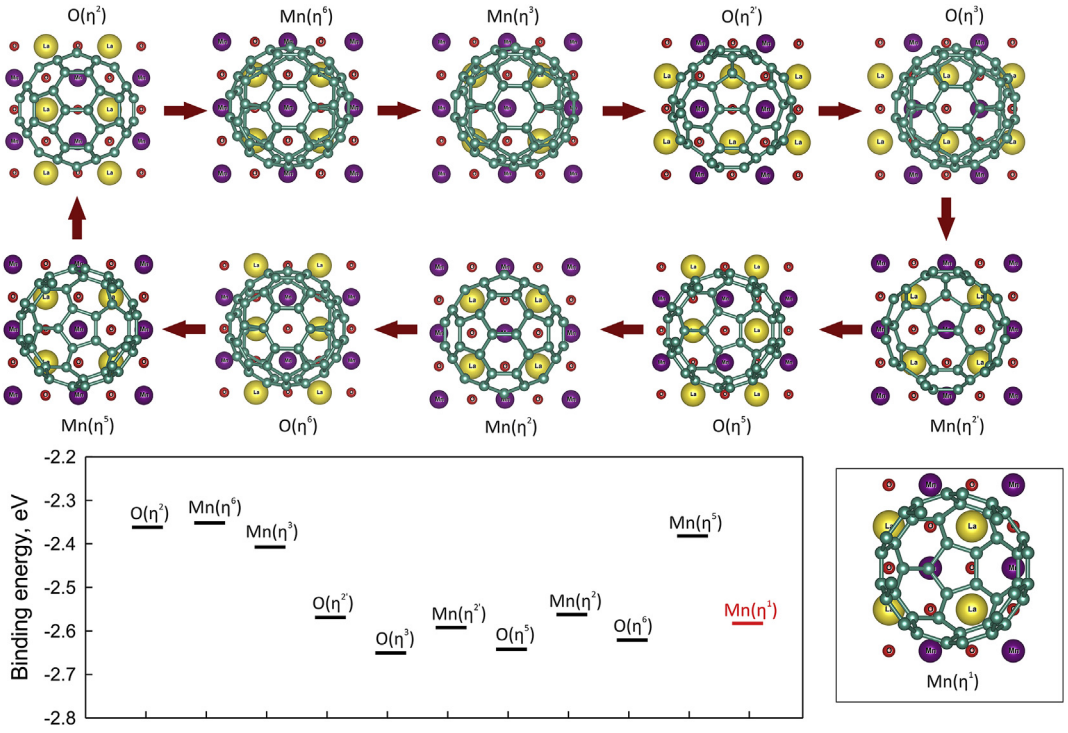

Fig. 1. Possible geometries of LSMO/C_{60} hybrid structures and binding energies corresponding to them. For the sake of better clarity, only the bottom part of the fullerene is presented, when needed. Inset shows additional structure with carbon atom placed upon Mn.

Table 1
Binding energy, fullerene's charge, magnetic moment and spin polarization at Fermi level in LSMO/C_{60} nanocomposites.

Type of structure	Binding energy, eV	C_{60} charge, e	C_{60} magnetic moment, μB	Spin polarization of C_{60} at Fermi level, %
Mn(η^6)	-2.3518	0.3261	0.0326	-4.7
Mn(η^5)	-2.3819	0.3361	0.0185	-13.7
Mn(η^2)	-2.5621	0.3389	0.0373	-6.6
Mn($\eta^{2'}$)	-2.5920	0.3661	0.0499	-20.1
Mn(η^3)	-2.4076	0.3340	0.0336	-5.9
O(η^6)	-2.6210	0.3603	0.0446	-13.0
O(η^5)	-2.6420	0.3698	0.0298	-21.9
O(η^2)	-2.3620	0.3165	0.0241	-3.8
O($\eta^{2'}$)	-2.5690	0.3544	0.0456	-11.0
O(η^3)	-2.6504	0.3703	0.0435	-18.3
Mn(η^1)	-2.5789	0.3576	0.0369	-24.5

approximately 0.36 e due to the interaction with LSMO slab, though it seems to be not spin-polarized according to the small value of magnetic moment (~0.04 μ_B). Spin density distribution analysis was then performed for two most favorable configurations (see Fig. 2). Only carbon atoms being placed upon Mn possess negative spin polarization while adjacent atoms are positively spin-polarized resulting in relatively small total magnetic moment on the molecule. This confirms our suggestions about the key role of Mn atoms in binding between fullerene and LSMO substrate.

In order to prove this, we then performed the calculation of one more additional structure with pentagon carbon atom being placed directly upon Mn atom (Mn(η^1) configuration, see inset on Fig. 1). Binding energy of this structure was found to lie in the range defined previously for structures with carbon upon manganese, though being lower than for O(η^3) and O(η^5) considered as the most favorable ones. This may be attributed to the fact that two manganese atoms are involved into the interaction in latter case (see Fig. 2) instead of one in case of Mn(η^1).

Properties of C_{60} molecule for this configuration are summarized in Table 1 and red-colored since they were not included when calculating averaged properties for Table 2. We additionally calculated probability of its appearance and found it to vary from 3 to 7% for different temperatures. Including this configuration into averaging procedure does not affect neither charge nor magnetic moment on fullerene molecule but increases the degree of spin polarization at Fermi level, especially at high temperatures. These new values are then presented in parentheses in Table 2. Indeed, one can clearly see from Table 1 that new Mn(η^1) structure

Table 2
Probability (P) of each configuration appearance, fullerene's averaged charge, magnetic moment and spin polarization versus temperature.

P				
	Temperature, K			
	300	400	500	600
Mn(η^6)	less than 0.01	less than 0.01	less than 0.01	less than 0.01
Mn(η^5)	less than 0.01	less than 0.01	less than 0.01	less than 0.01
Mn(η^2)	0.01	0.03	0.04	0.06
Mn($\eta^{2'}$)	0.05	0.07	0.09	0.10
Mn(η^3)	less than 0.01	less than 0.01	less than 0.01	less than 0.01
O(η^6)	0.14	0.17	0.17	0.18
O(η^5)	0.32	0.30	0.29	0.27
O(η^2)	less than 0.01	less than 0.01	less than 0.01	less than 0.01
O($\eta^{2'}$)	0.02	0.03	0.05	0.06
O(η^3)	0.45	0.39	0.35	0.32
Averaged properties of C_{60} molecule				
	Temperature, K			
	300	400	500	600
Charge, e	0.3677	0.3666	0.3658	0.3648
Magnetic moment, μB	0.0394	0.0398	0.0401	0.0403
Spin polarization at Fermi level, %	-18.5 (-18.6)	-18.0 (-18.3)	-17.6 (-18.0)	-17.3 (-17.8)

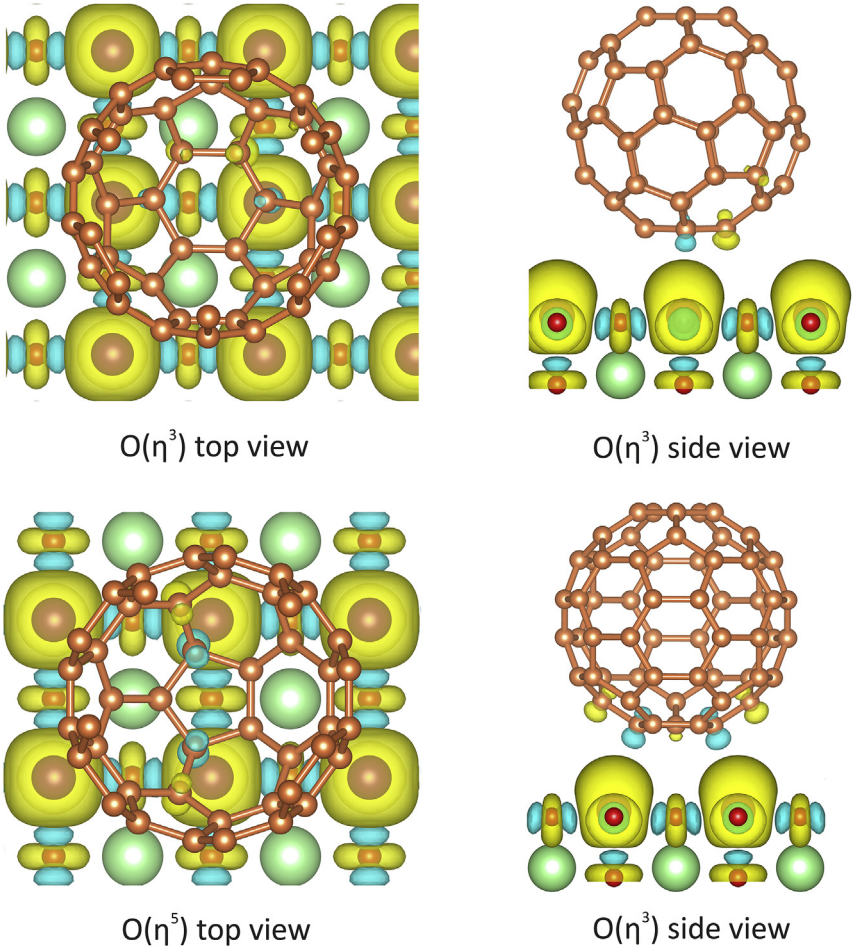

Fig. 2. Spatial spin density distribution in LSMO/C_{60} composites. Blue and yellow areas denote spin-up and spin-down density, respectively. (For interpretation of the references to colour in this figure legend, the reader is referred to the web version of this article).

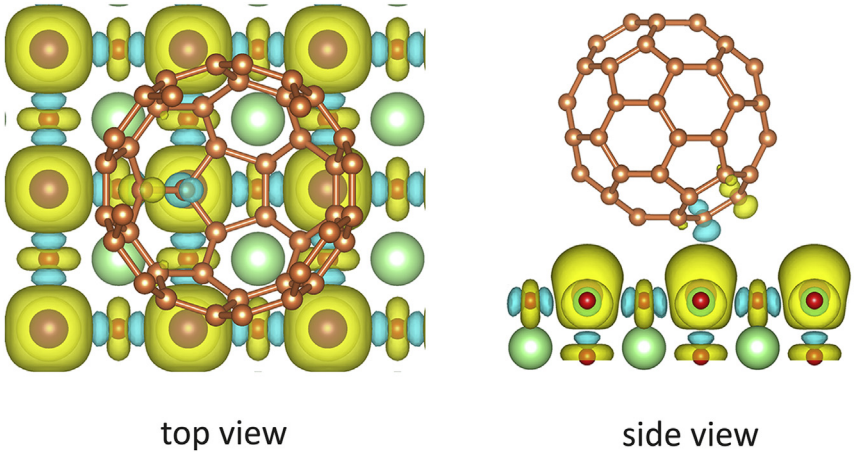

Fig. 3. Spatial spin density distribution for Mn(η [1]) structure. Blue and yellow areas denote spin-up and spin-down density, respectively. (For interpretation of the references to colour in this figure legend, the reader is referred to the web version of this article).

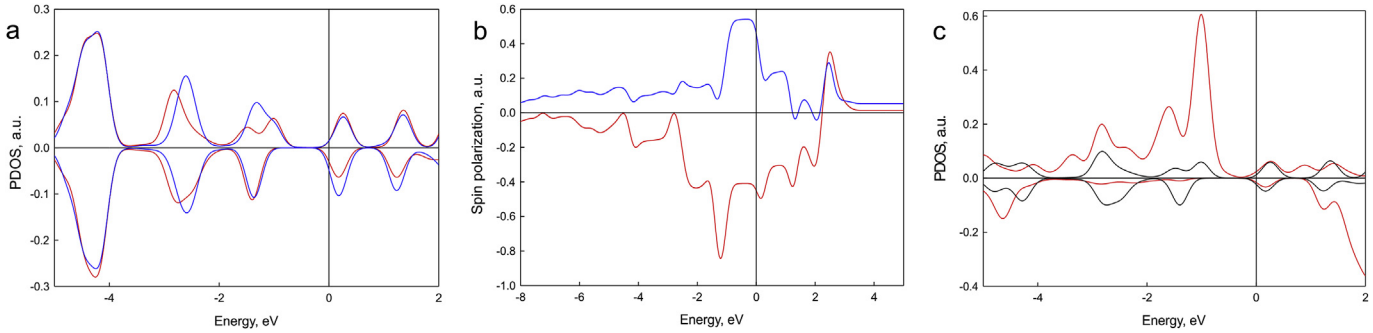

Fig. 4. Partial density of states (a) and overall spin polarization (b) for C atom contacting with Mn (red line) and adjacent C atom (blue line); partial density of states (c) for Mn d_{z^2} (red line) and carbon p_z (black line) orbitals. (For interpretation of the references to colour in this figure legend, the reader is referred to the web version of this article).

possesses the highest degree of spin polarization among all. Spin density spatial distribution presented on Fig. 3 is in perfect agreement with results previously obtained (see Fig. 2).

However, analysis of PDOS plotted for positively and negatively spin-polarized carbon atoms shows only the minor difference between them (see Fig. 4a). Higher spin polarization at Fermi level for C atom adjacent to contacting is also quite puzzling and complicates the understanding of physics beyond this. This problem can be solved by integrating the DOS over the energies (which corresponds to how many states can be found below the given energy) and then taking the residual between spin-up and spin-down integrated DOS which gives the total spin polarization itself. Such analysis is presented on Fig. 4b. Apparently, Mn atom affects contacting C atom making it negatively spin-polarized, and contacting C, in turn, affects adjacent carbon atom resulting into positive spin polarization of the latter. This can be seen from the perfect match between all the features in their spin polarization spectra. The abovementioned kind of magnetic ordering then spreads over the whole C_{60} molecule with decreasing intensity and can be seen from spatial spin density patterns when lowering isosurface level. In fact, complex magnetic exchange mechanism is involved. It appears to be very similar to superexchange interaction between 3d metal cations and nonmagnetic anions but here the overlapping between manganese d_{z^2} orbitals and molecular orbitals of C_{60} molecule takes place (see Fig. 4c). This gives us insight of how spin-polarized current flows through LSMO/C_{60} interface though the total magnetic moment of fullerene molecule is considerably low.

4. Conclusions

In conclusion, we investigated atomic and electronic structure of LSMO/C_{60} nanocomposite and found many possible structures to co-exist in wide range of temperatures. Only spin polarization at Fermi level was found to depend strongly on the configuration while both C_{60} charge and magnetic moment remain virtually the same. However, spin-polarized transport is still possible even for less favorable configurations. Manganese atoms play a key role in binding between fullerene and LSMO which is confirmed by the values of binding energies and spatial spin density distribution patterns. The mechanism of spin-polarized charge transport was discussed. According to our analysis of magnetic moment values and spin density spatial distribution, it's evident that this is due to the special kind of magnetic ordering in C_{60} molecule rising from the interaction with manganese atoms and complex magnetic exchange interaction.

Acknowledgements

This work was supported by the Russian Scientific Fund (Project No. 14-13-00139). The authors would like to thank Institute of Computational Modeling of SB RAS, Krasnoyarsk; Joint Supercomputer Center of RAS, Moscow; Center of Equipment for Joint Use of Siberian Federal University, Krasnoyarsk; ICC of Novosibirsk State University and Siberian Supercomputer Center (SSCC) of SB RAS, Novosibirsk for providing the access to their supercomputers.

References

[1] W.J.M. Naber, S. Faez, W.G. van der Wiel, W.G. Van Der Wiel, J. Phys. D Appl. Phys. 40 (2007) R205.
[2] V. Dediu, M. Murgia, F.C. Matacotta, C. Taliani, S. Barbanera, Solid State Commun. 122 (2002) 181.
[3] V.A. Dediu, L.E. Hueso, I. Bergenti, C. Taliani, Nat. Mater. 8 (2009) 707.
[4] T.D. Nguyen, G. Hukic-Markosian, F. Wang, L. Wojcik, X.-G. Li, E. Ehrenfreund, Z.V. Vardeny, Nat. Mater. 9 (2010) 345.
[5] Z.H. Xiong, D. Wu, Z.V. Vardeny, J. Shi, Nature 427 (2004) 821.
[6] V. Dediu, L.E. Hueso, I. Bergenti, A. Riminucci, F. Borgatti, P. Graziosi, C. Newby, F. Casoli, M.P. De Jong, C. Taliani, Y. Zhan, Phys. Rev. B Condens. Matter Mater. Phys. 78 (2008) 115203.
[7] C. Barraud, P. Seneor, R. Mattana, S. Fusil, K. Bouzehouane, C. Deranlot, P. Graziosi, L. Hueso, I. Bergenti, V. Dediu, F. Petroff, A. Fert, Nat. Phys. 6 (2010) 615.
[8] J.J.H.M. Schoonus, P.G.E. Lumens, W. Wagemans, J.T. Kohlhepp, P.A. Bobbert, H.J.M. Swagten, B. Koopmans, Phys. Rev. Lett. 103 (2009).
[9] M. Gobbi, A. Pascual, F. Golmar, R. Llopis, P. Vavassori, F. Casanova, L.E. Hueso, Org. Electron. Phys. Mater. Appl. 13 (2012) 366.
[10] M. Gobbi, F. Golmar, R. Llopis, F. Casanova, L.E. Hueso, Adv. Mater. 23 (2011) 1609.
[11] F. Li, T. Li, F. Chen, F. Zhang, Org. Electron. Phys. Mater. Appl. 15 (2014) 1657.
[12] F. Li, ACS Appl. Mater. Interfaces 5 (2013) 8099.
[13] R. Lin, F. Wang, M. Wohlgenannt, C. He, X. Zhai, Y. Suzuki, Synth. Met. 161 (2011) 553.
[14] S. Liang, R. Geng, B. Yang, W. Zhao, R. Chandra Subedi, X. Li, X. Han, T.D. Nguyen, Sci. Rep. 6 (2016) 19461.
[15] J. Krempaský, V.N. Strocov, L. Patthey, P.R. Willmott, R. Herger, M. Falub, Phys. Rev. B 77 (2008) 165120.
[16] B. Nadgorny, J. Phys. Condens. Matter 19 (2007) 315209.
[17] T.D. Nguyen, F. Wang, X.-G. Li, E. Ehrenfreund, Z.V. Vardeny, Phys. Rev. B 87 (2013) 075205.
[18] H. Xie, D. Niu, L. Lyu, H. Zhang, Y. Zhang, P. Liu, P. Wang, D. Wu, Y. Gao, Appl. Phys. Lett. 108 (2016) 011603.
[19] G. Kresse, J. Furthmüller, Comput. Mater. Sci. 6 (1996) 15.
[20] G. Kresse, J. Furthmüller, Phys. Rev. B 54 (1996) 11169.
[21] G. Kresse, J. Hafner, Phys. Rev. B 47 (1993) 558.
[22] G. Kresse, J. Hafner, Phys. Rev. B 49 (1994) 14251.
[23] J.P. Perdew, J.A. Chevary, S.H. Vosko, K.A. Jackson, M.R. Pederson, D.J. Singh, C. Fiolhais, Phys. Rev. B 46 (1992) 6671.
[24] J.P. Perdew, J.A. Chevary, S.H. Vosko, K.A. Jackson, M.R. Pederson, D.J. Singh, C. Fiolhais, Phys. Rev. B 48 (1993) 4978.
[25] V.I. Anisimov, J. Zaanen, O.K. Andersen, Phys. Rev. B 44 (1991) 943.
[26] S.L. Dudarev, S.Y. Savrasov, C.J. Humphreys, A.P. Sutton, Phys. Rev. B 57 (1998) 1505.
[27] P.E. Blöchl, Phys. Rev. B 50 (1994) 17953.
[28] G. Kresse, Phys. Rev. B 59 (1999) 1758.
[29] S. Grimme, J. Comput. Chem. 27 (2006) 1787.
[30] C. Ma, Z. Yang, S. Picozzi, J. Phys. Condens. Matter 18 (2006) 7717.
[31] S. Picozzi, C. Ma, Z. Yang, R. Bertacco, M. Cantoni, A. Cattoni, D. Petti, S. Brivio, F. Ciccacci, Phys. Rev. B 75 (2007) 94418.
[32] B. Zheng, N. Binggeli, Phys. Rev. B 82 (2010) 245311.
[33] M.C. Martin, G. Shirane, Y. Endoh, K. Hirota, Y. Moritomo, Y. Tokura, Phys. Rev. B 53 (1996) 14285.
[34] F. Tsui, M.C. Smoak, T.K. Nath, C.B. Eom, Appl. Phys. Lett. 76 (2000) 2421.
[35] H.J. Monkhorst, J.D. Pack, Phys. Rev. B 13 (1976) 5188.
[36] W. Tang, E. Sanville, G. Henkelman, J. Phys. Condens. Matter 21 (2009) 084204.
[37] E. Sanville, S.D. Kenny, R. Smith, G. Henkelman, J. Comput. Chem. 28 (2007) 899.
[38] G. Henkelman, A. Arnaldsson, H. Jónsson, Comput. Mater. Sci. 36 (2006) 354.
[39] H. Nejat Pishkenari, A. Nemati, A. Meghdari, S. Sohrabpour, Curr. Appl. Phys. 15 (2015) 1402.
[40] A.A. Kuzubov, E.A. Kovaleva, P.V. Avramov, A.S. Kholtobina, N.S. Mikhaleva, A.V. Kuklin, J. Magn. Magn. Mater. 410 (2016) 41–46.